Method

Fabian

30/04/2021

Method

Summary

- Workflows to calculate biomass from FIA plots (Shana) are in practice (Hudak et al., 2020)
- Landtrendr (Landsat, Google Earth) can be used to study forest regeneration patterns via normalised burn ratio (NBR) over large time intervals (30 years). Data can be used to estimate damage in areas which take longer to recover.

Sentinel 2

Compared to Landsat multispectral bands, the Sentinel-2 multispectral bands provide two red edge bands and one NIR band with improved spatial resolution. The Sentinel 2 bands can be used to derive various vegetation indices useful for discriminating between species and estimating forest biomass (Tab. 1)

Table. 1: Overview Sentinel 2 bands (Arcgis.com)

Band	Description	Wavelength..um.	Resolution..m.
1	Coastal Aerosol	0.433 - 0.453	60
2	Blue	0.458 - 0.523	10
3	Green	0.543 - 0.578	10
4	Red	0.650 - 0.680	10
5	RE1	0.698 - 0.713	20
6	RE2	0.733 - 0.748	20
7	RE3	0.773 - 0.793	20
8	NIR	0.785 - 0.900	10
8a	Narrow NIR	0.855 - 0.875	20
9	Water vapour	0.935 - 0.955	60
10	SWIR-Cirrus	1.365 - 1.385	60
11	SWIR-1	1.565 - 1.655	20
12	SWIR-2	2.100 - 2.280	20

Vegetation Indices

Vegetation indices including near-infrared wavelength have weaker relationships with biomass than those including shortwave infrared wavelength, especially for forest sites with complex stand structures. The results of image transformations such as the first principal component from the PCA showed stronger relationships with biomass than individual spectral bands, somehow independent of different biophysical conditions. However, in a study area with poor soil conditions and relatively simple forest stand structure, near-infrared band or relevant vegetation indices had a strong relationship with biomass (Lu et al., 2016)

Table. 2: Vegetation Indices derived from Sentinel 2 information (after Pandit et al., 2018)

Vegetation.Indices	Equations	References
NDVI	(NIR - R/NIR + R)	(Tucker 1979)
RGR (Red Green Ratio)	Red665/Green560	(Sims & Gamon 2002)
EVI (Enhanced Vegetation Index)	2.5*((NIR - R)/ (1 + NIR + 6R - 7.5 Blue))	(A. Huete et al. 2002)
SR (Simple ratio)	NIR/RED	(Jordan 1969)
PSRI (Plant Senescence Reflectance Index)(665 - 560/740)	(Hill 2013; Merzlyak et al. 1999)	
NDII (Normalized Difference Infrared Index)	(842 - 1610/842 + 1610)	(Hardisky et al. 1983)
RE NDVI	842 - 740/842 + 740	(Chen et al. 2007)
SAVI (Soil-Adjusted Vegetation Index)	(NIR - R)/(NIR + R + L)*1.5	(Huete 1988)
RECI (Inverted Red-Edge Chlorophyll Index)	NIR - R/(RE1/RE2)	(Frampton et al. 2013)
Sentinel-2-red-edge position	[705 + 35*(0.5*(B7 + B4)/2) - B5)/(B6 - B5)]	(Frampton et al. 2013)
Red-edge-based NVDI's		
1	(NIR - RE1/NIR + RE1)	(Kross et al. 2015)
2	(NIR - RE2/NIR + RE2)	(Gitelson & Merzlyak 1994; Kross et al. 2015)
3	(NIR - RE3/NIR + RE3)	(Sharma et al. 2015)
4	(NIR - RE4/NIR + RE4)	(Kross et al. 2015)

Papers:
Estimating ABG in sub-tropical Nepal using Sentinel 2 (Pandit et al., 2018). Field-based AGB as a dependent variable, as well as spectral band values and spectral-derived vegetation indices as independent variables in the Random Forest (Breiman, 2001). In this algorithm, decision trees are generated to the maximum extent without pruning using a randomly-selected two thirds of the samples as training data with bootstrapping (re-sampling the data many times with replacement), which strengthens the flexibility by aggregating the prediction across individual trees to make a final prediction. The paper ranks importance of spectral band data and vegetation indices from above (Tab. 1) as a typical output of a random forest. (R2 = 0.81 and RMSE = 25.57 t ha-1).

Normalised Burn Ratio

The NBR index has been traditionally used to map burn severity [63]. However, recently, it also has been used to assess forest disturbances, such as those caused by selective logging (Shimizu et al., 2017). (Lima et al. 2019)

The Normalized Burn Ratio (NBR) is an index designed to highlight burnt areas in large fire zones. The formula is similar to NDVI, except that the formula combines the use of both near infrared (NIR) and shortwave infrared (SWIR) wavelengths (Fig 1).

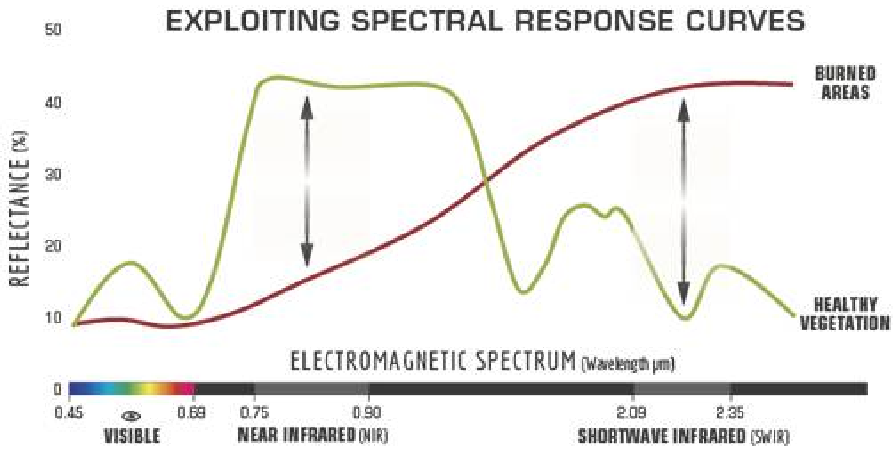

Fig: 1 Comparison of the spectral response of healthy vegetation and burned areas (USFS)

NBR uses the ratio between NIR and SWIR bands, according to the formula shown below. A high NBR value indicates healthy vegetation while a low value indicates bare ground and recently burnt areas. Non-burnt areas are normally attributed to values close to zero.

NBR = (NIR-SWIR)/(NIR+SWIR)

Burn severity can then be estimated from the difference between pre- and post-fire NBR.

Papers:

Sentinel 2 data to create fire database in sub-Saharan Africa (Roteta et al., 2019). Sentinel-2 MSI reflectance measurements in the short and near infrared wavebands plus the activefires detected by Terra and Aqua MODIS sensor. They were able to detect smaller fires than with common MODIS approach, but Sentinel-2 based products have lower temporal resolution and consequently are more affected by cloud/cloud shadows. Available here: https://climate.esa.int/en/projects/fire/data/

Fire on Madeira, Spain (Navarro et al., 2017). Sentinel-2 data (5 days, 10 m resolution) for pre- and post-fire image assessments (sometimes just two). The framework can be used for the assessment of many other burnt areas globally. Enabling an extremely unprecedented perspective with a unique set of accurate, robust, timely and easily accessible information. No real measurement of accuracy provided.

Problems with Sentinel 2 Data

Papers: Bamboo forest in China: Seasonality, different growth phenomena in different years. Correlation between spectral bands and biomass varies within the period of months. Biomass calculation based on DBH and age (Y. Chen et al., 2019). Also used random forest to evaluate key variables.

LiDAR

Jonathan Kane(meeting 29 April): We assume > 2m can be classified as canopy.

LiDAR for biomass quantification.

Recent paper with Jonathan and Van Kane (Hudak et al. 2020). Used a Carbon Monitoring System (CMS) to produce annual estimates of aboveground biomass using Random Forests (RF). Field plots collected by the US Forest Service and other in northwestern USA. Plot level AGB estimates were used as a response variable to predict AGB from LiDAR derived canopy height and density information ($R2 = 0.8$, RMSE =

115 Mg ha-1, Bias = 2 Mg ha-1). A stratified random sample of AGB pixels from these landscape-level AGB maps then served as training data for predicting AGB regionally from Landsat image time series variables processed through LandTrendr. Climate metrics calculated from downscaled 30 year climate normals were used as predictors for both models (landscape and regional), as were topographic metrics calculated from elevation data; these environmental predictors allowed AGB estimation over the full range of observations with the regional model (R2 = 0.8, RMSE = 152 Mg ha-1, Bias = 9 Mg ha-1), including higher AGB values (>400 Mg ha-1) where spectral predictors alone saturate.

Found both our project landscape and regional, annual AGB estimates to be unbiased with respect to FIA estimates (Biases of 1% and 0.7%, respectively)

Combination of LiDAR and other imagery for biomass estimation

Long-standing research question in lidar remote sensing for AGB estimation is to understand whether the addition of passive optical imagery to airborne lidar can further improve AGB modeling performance (Dengsheng Lu et al., 2016).

Combination of lidar and QuickBird image did not improve AGB estimation in mixed coniferous forests in California; lidar data alone provided a better performance (Hyde et al., 2006)

LiDAR and hyperspectral combination has lower accuracy than LiDAR alone in tropical forest Costa Rica (Clark et al., 2011).

As a result research has shifted to use non-parametric algorithms such as KNN, artificial neural network, support vector regression (SVR) and random forest (RF).

Field data

Shana sampling plots

Applications of LiDAR for forest inventory require further investment into field plot data collections to estimate most stand attributes of interest (volume, basal area, biomass, etc.) (Hudak et al., 2020)

s. However, the caveat is that they collectively represent a spatially biased sample of forests in the region. This is a key distinction of our project datasets from FIA plot data, which provide an unbiased, systematic sample of forest conditions in space and time, as is needed in support of forest planning and monitoring, reporting, and verification (MRV) (Tinkham et al 2018, Hurtt et al 2019).

Sampling plot data from the Forest Inventory and Analysis National Program (FIA). Sampling plots are available

- Allometric: DBH, size classes (e.g. saplings) > height groups, largest tree measured, height to live crown, crown ratio, crown width, age data sparse and based on 1-2 cores
- Biomass derived from LiDAR datasets
- plot center GPS using Javad
- plot date and size
- Ancillary data: Slope, ground cover, vegetation cover by type (e.g. shrub, forb, etc), modal vegetation height by different types of vegetation, fuel models, fuels data, seedlings, site history (e.g. plantation, if there was a fire, etc)

Van Kane (meeting Apr 29): Forest plots are triangle with 4 circular subplots, just pretend they are representative of 1 ha of forest

Sampling techniques used: https://www.fia.fs.fed.us/program-features/index.php

Spatial mismatch between the 7.3 m radius, round configuration of an FIA subplot and 30 m × 30 m square Landsat pixels (Tinkham et al 2018). Inevitably, the four subplots will intersect a different number of pixels and in varying proportions (Fig. 2, Hudak et al., 2020)

Depending on the protocol and the quality of the Global Navigation Satellite System (GNSS) receiver used in the field; the three peripheral subplots, while systematically laid out from the center subplot by consistent distances (36.6 m) and bearings (120 ∘ , 240 ∘ , 360 ∘) are usually not georeferenced, making them more subject to locational inaccuracy due to additive errors in accounting for horizontal distance on slopes and for magnetic declination on compass azimuths (Zald et al 2014).

Criteria to match LiDAR with FIA plots (Hudak et al., 2020):

- fixed-area plots
- georeferenced with a GNSS capable of differential correction
- established within ±3 years of an overlapping lidar collection
- not disturbed in the time between field and lidar data collections

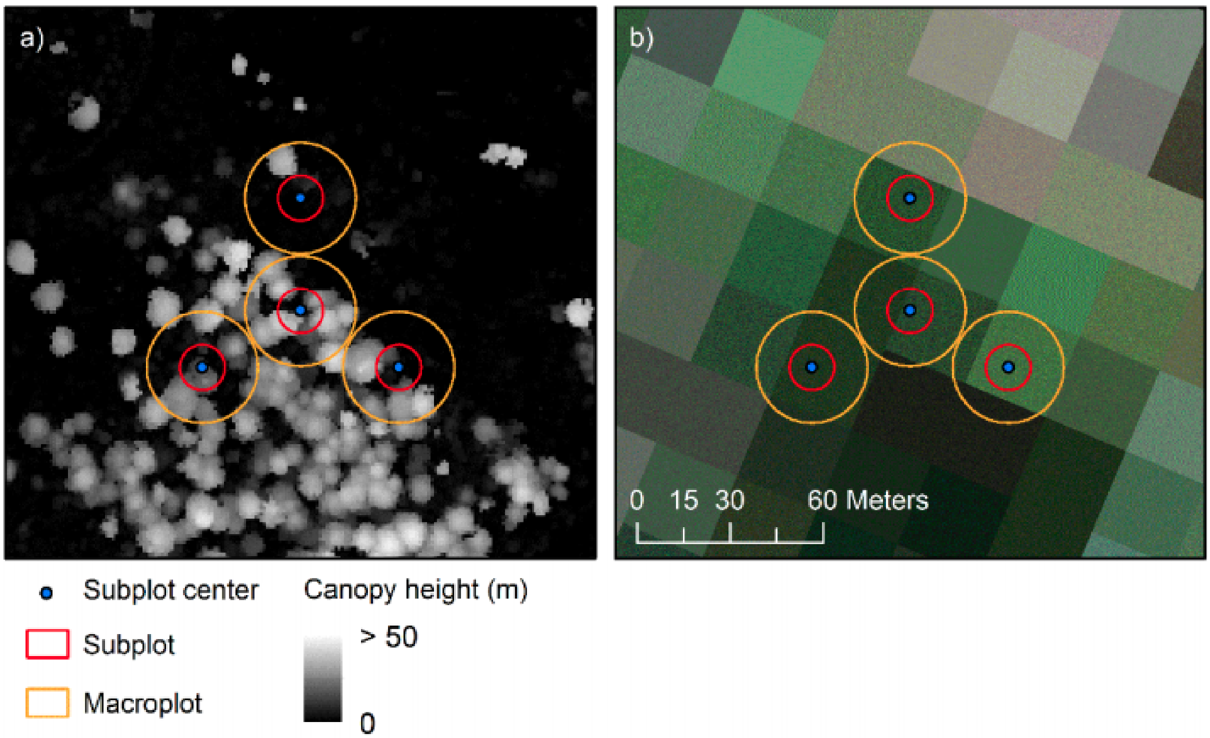

Figure 2: FIA sampling plot layout. a) generated canopy height model from lidar and b) landsat 30m imagery overlay (taken from Hudak et al., 2020)

Biomass estimation in the field

Collection of a large number of biomass reference data at the plot level is time-consuming and labor-intensive. It is only suitable for a small area and cannot provide the spatial distribution. However, this kind of data is a prerequisite for developing biomass estimation models (Lu et al., 2016). Allometric models most common, but require data about soil, land use history and climate influence (paper here for tropical) (Clark & Kellner, 2012).

(table Lu et al 2016)

Use data of national forest inventories:

ABG (kg/ha) = volume (m3 / ha) * VEF * WD * BEF +

with volume expansion factor (VEF), average wood density (WD), biomass expansion factor (BEF) (Brown et al., 1989; Lehtonen et al., 2004; Wang et al., 2011)

(Hudak et al., 2020): AGB was calculated from project field plot tree measurements using the default equations found in local variants of the Fire and Fuels Extension (FFE) of the Forest Vegetation Simulator

(FVS) (Rebain 2015, Dixon 2018). These equations are based on a series of regional volume and biomass equations. The aboveground portion of the live and standing dead trees were summed to a single, plot-level AGB value; the belowground portion of the trees and non-tree species were excluded from the AGB estimates. These plot-level AGB estimates were the response variable for the landscape model

Problems with field data

(1) tree variables, including sampling, measurement, recording and grouping errors when tree variables such as DBH and height are measured;
(2) conversion coefficients and models including variation of conversion factors from volume to biomass and then to carbon, inappropriate selection and usage of allometric models for relationship of tree volume and DBH and height, and incorrect regression models relating forest biomass/carbon to spectral variables;
(3) uncertainties of spectral values due to unbalanced platforms, scanner motions, poor atmospheric conditions, and slope; inappropriate spatial interpolation methods for geometrical and radiometric corrections, and incorrect methods for image enhancement and analysis;
(4) sample plot locations, including global positing system (GPS) coordinates used to locate the sample plots, geometric correction and the uncertainties due to mismatch of sample plots with spatial resolutions of remotely sensed data;
(5) differences in sizes of sample plots and image pixels, disagreement between remotely sensed data and plot observations when portions of trees on boundaries are outside plots although both sample plots and pixels have the same spatial resolutions; and
(6) temporal differences between field plot measurements and remotely sensed data.

Forest classification

Van Kane (meeting Apr 29): forest service cannot reveal plot locations, only if project output is open access (ideally uni projects) Idea: Use Gradient nearest neighbours (GNN) so nearest plot imputes tree list

Landsat

Table. 3: Landsat 8-9 Operational Land Imager (OLI) and Thermal Infrared Sensor (TIRS) (USGS)

Bands	Wavelength..um.	Resolution..m.
Band 1- Coastal aerosol	0.43-0.45	30
Band 2- Blue	0.45-0.51	30
Band 3- Green	0.53-0.59	30
Band 4- Red	0.64-0.67	30
Band 5- Near Infrared (NIR)	0.85-0.88	30
Band 6- SWIR 1	1.57-1.65	30
Band 7- SWIR 2	2.11-2.29	30
Band 8- Panchromatic	0.50-0.68	15
Band 9- Cirrus	1.36-1.38	30
Band 10- Thermal Infrared (TIRS) 1	10.6-11.19	100
Band 11- Thermal Infrared (TIRS) 2	11.50-12.51	100

Hudak 2020: However, the 30 m resolution of Landsat TM is less than satisfying to land managers that seek to make operational decisions at the local level. Moreover, Landsat and for that matter all passive optical imagery suffers from lack of sensitivity in cases of high canopy closure (Smith et al 2009) or in high biomass forests, with the signal saturating at an AGB density of ~150– 250 Mg ha-1 or more depending on the study (Huete et al 1997, Steininger 2000, Dong et al 2003, Avitabile et al 2012, Zhu and Liu 2015, Durante et al 2019).

LandTrendr is set of spectral-temporal segmentation algorithms that are useful for change detection in a time series of moderate resolution satellite imagery (primarily Landsat) and for generating trajectory-based spectral time series data largely absent of inter-annual signal noise. Can be used to assess forest regeneration over larger timescales (Fig. 3). They provide a github repository evaluating how to extract the data from Google Earth (https://emapr.github.io/LT-GEE/landtrendr.html).

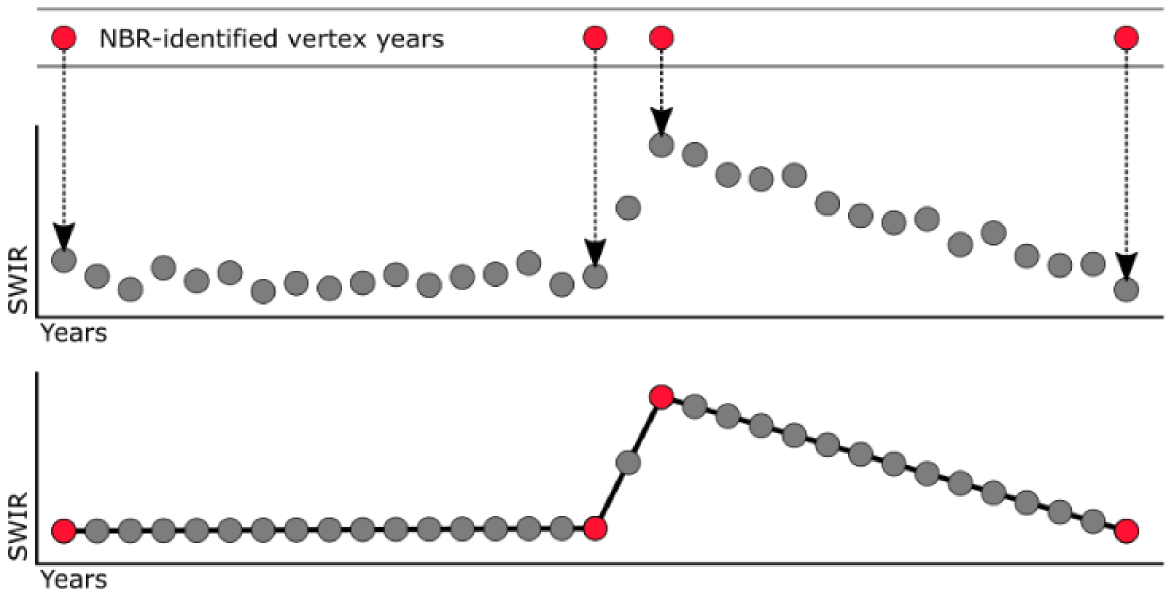

Fig 2.4. Impose the segmentation structure of one spectral representation on another. Here we have identified four breakpoints or vertices for a pixel time series using NBR, and then used the year of those vertices to segment and interpolate the values of a SWIR band time series for the same pixel.

Figure 3: Normalised Burn Ratio (NBR)

Papers: Jonathan Kane paper (Kolden et al., 2012). We characterized unburned area within fire perimeters by fire size and severity, characterized distance to an unburned area across the burned portion of the fire, and investigated patch dynamics of unburned patches within the fire perimeter. From 1984 through 2009, the total area within the fire perimeters that was classified as unburned from dNBR was 37% for Yosemite, 17% for Glacier, and 14% for Yukon-Charley.
The complex biophysical environments and vegetation characteristics, e.g. phenology, species composition, growth phase, and health – will affect vegetation spectral signatures; thus, biomass estimation models based on optical spectral features cannot be directly transferred to different study areas for biomass mapping (Foody et al., 2003; Lu, 2005)

Synthetic aperture radar (SAR)

Most radar-based biomass estimation studies use L-band SAR data, especially the ALOS PALSAR L-band data (Mitchard et al. 2011; Carreiras et al. 2012; Rahman and Sumantyo 2013). The SAR C-band data have not been extensively used because of the C-band's inability to capture forest biomass features (Le Toan et al. 1992; Lu 2006).

In summary, it is difficult to use radar data for distinguishing vegetation types (Li et al. 2012b) because radar data reflect the roughness of land cover surfaces instead of the difference between the vegetation types, thus resulting in difficulty of biomass estimation. The speckle in radar data is another problem affecting its applications. Properly employing filtering methods to reduce noise and outliers in InSAR data is needed to improve the vegetation height estimation performance (Kellndorfer et al. 2004).

RapidEye

ESA is offering access to the full RapidEye archive for scientific research and application development. Access is only available to submitted proposals that are accepted.

Type High-resolution optical imager Resolution (IFOV) 6.5m GSD at nadir, resampled to 5 m pixel size on orthorectified products Swath Width (FOV) ± 6.75º about nadir, corresponding to a swath of 77 km Bands Blue 440-510 nm Green 520-590 nm Red 630-685 nm Red edge 690-730 nm NIR (Near Infrared) 760-850 nm

Overall, RapidEye data are not suitable for AGB estimation, but when AGB falls within 50–150 Mg/ha, support vector regression based on stratification of vegetation types provided good AGB estimation; Problem for biomass estimates can be fixed incorporating tree height if LiDAR data or stereo image is available (Brasilian Rainforest) (Feng et al., 2017)

ICESat-2

Ice, Cloud and Land Evalutation Satellite, 91-day repeat
While ATLAS onboard ICESat-2 was primarily designed to determine changes in ice sheet elevation and mass, it will provide information about vegetation that may be used to estimate AGB. ATLAS is a photon counting system, operating in the visible wavelengths, at 532 nm [7]. It generates three pairs of tracks, with each pair approximately 3.3 km apart and each track within a pair separated by 90 m [11]. Lidar footprints are produced every 70 cm in the along-track direction and measure approximately 14 m in diameter [14]. Given the unprecedented coverage and spatial detail from ICESat-2, translating ICESat-2 measurements to AGB estimates would allow for large-scale AGB and forest carbon assessments.

Paper: ICESat-2 for mapping forest biomass with deep learning (Narine et al., 2019). A first set of models were developed using vegetation indices calculated from single-date Landsat imagery, canopy cover, and land cover, and a second set of models were generated using metrics from one year of Landsat imagery with canopy cover and land cover maps. With the extended dataset containing metrics calculated from Landsat images acquired on different dates, substantial improvements in modelperformance for all data scenarios were noted. The R2 values increased to 0.64, 0.66, and 0.67. Comparisons with Random forest (RF) prediction models highlighted similar results, with the same R2 and root mean square error (RMSE) range (15–16 Mg/ha) for daytime and nighttime scenarios. ICESat-2 profiles, especially with the nighttime scenario (R2 = 0.66), highlight the potential for generating a wall-to-wall AGB product with ICESat-2 by adopting a synergistic approach with Landsat optical imagery, canopy cover, and land cover

References

ArcGIS.com. (2021). Sentinel-2 Imagery: Normalized Burn Ratio—Overview. https://www.arcgis.com/home/item.html?id=5cbafcf777e845129771e601701aaae7

Breidenbach, J., Næsset, E., Lien, V., Gobakken, T., & Solberg, S. (2010). Prediction of species specific forest inventory attributes using a nonparametric semi-individual tree crown approach based on fused airborne laser scanning and multispectral data. Remote Sensing of Environment, 114, 911–924. https://doi.org/10.1016/j.rse.2009.12.004

Breiman, L. (2001). Random Forests. Machine Learning, 45(1), 5–32. https://doi.org/10.1023/A:1010933404324

Broge, N. H., & Leblanc, E. (2001). Comparing prediction power and stability of broadband and hyperspectral vegetation indices for estimation of green leaf area index and canopy chlorophyll density. Remote Sensing of Environment, 76(2), 156–172. https://doi.org/10.1016/S0034-4257(00)00197-8

Brown, S., Gillespie, A., & Lugo, A. (1989). Biomass Estimation Methods for Tropical Forests with Applications to Forest Inventory Data. Forest Science, 35, 881–902.

Chen, J.-C., Yang, C.-M., Wu, S.-T., Chung, Y.-L., Charles, A. L., & Chen, C.-T. (2007). Leaf chlorophyll content and surface spectral reflectance of tree species along a terrain gradient in Taiwan's Kenting National Park. 48, 71–77.

Chen, Q., Baldocchi, D., Gong, P., & Kelly, M. (2006). Isolating Individual Trees in a Savanna Woodland using Small Footprint LIDAR data. Photogrammetric Engineering and Remote Sensing, 72, 923–932. https://doi.org/10.14358/PERS.72.8.923

Chen, Y., Li, L., Lu, D., & Li, D. (2019). Exploring Bamboo Forest Aboveground Biomass Estimation Using Sentinel-2 Data. Remote Sensing, 11(1), 7. https://doi.org/10.3390/rs11010007

Clark, D. B., & Kellner, J. R. (2012). Tropical forest biomass estimation and the fallacy of misplaced concreteness. Journal of Vegetation Science, 23(6), 1191–1196. https://doi.org/10.1111/j.1654-1103.2012.01471.x

Clark, M. L., Roberts, D. A., Ewel, J. J., & Clark, D. B. (2011). Estimation of tropical rain forest aboveground biomass with small-footprint lidar and hyperspectral sensors. Remote Sensing of Environment, 115(11), 2931–2942. https://doi.org/10.1016/j.rse.2010.08.029

Curran, P. J. (2001). Imaging spectrometry for ecological applications. International Journal of Applied Earth Observation and Geoinformation, 3(4), 305–312. https://doi.org/10.1016/S0303-2434(01)85037-6

Feng, Y., Lu, D., Chen, Q., Keller, M., Moran, E., dos-Santos, M. N., Bolfe, E. L., & Batistella, M. (2017). Examining effective use of data sources and modeling algorithms for improving biomass estimation in a moist tropical forest of the Brazilian Amazon. International Journal of Digital Earth, 10(10), 996–1016. https://doi.org/10.1080/17538947.2017.1301581

Foody, G. M., Boyd, D. S., & Cutler, M. E. J. (2003). Predictive relations of tropical forest biomass from Landsat TM data and their transferability between regions. Remote Sensing of Environment, 85(4), 463–474. https://doi.org/10.1016/S0034-4257(03)00039-7

Frampton, W. J., Dash, J., Watmough, G., & Milton, E. J. (2013). Evaluating the capabilities of Sentinel-2 for quantitative estimation of biophysical variables in vegetation. ISPRS Journal of Photogrammetry and Remote Sensing, 82, 83–92. https://doi.org/10.1016/j.isprsjprs.2013.04.007

Gitelson, A., & Merzlyak, M. N. (1994). Spectral Reflectance Changes Associated with Autumn Senescence of Aesculus hippocastanum L. and Acer platanoides L. Leaves. Spectral Features and Relation to Chlorophyll Estimation. Journal of Plant Physiology, 143(3), 286–292. https://doi.org/10.1016/S0176-1617(11)81633-0

Gleason, C. J., & Im, J. (2011). A Review of Remote Sensing of Forest Biomass and Biofuel: Options for Small-Area Applications. GIScience & Remote Sensing, 48(2), 141–170. https://doi.org/10.2747/1548-1603.48.2.141

Hardisky, M., Klemas, V., & Smart, and. (1983). The influence of soil salinity, growth form, and leaf moisture on the spectral radiance of Spartina Alterniflora canopies. Photogrammetric Engineering and Remote Sensing, 48, 77–84.

Hill, M. J. (2013). Vegetation index suites as indicators of vegetation state in grassland and savanna: An analysis with simulated SENTINEL 2 data for a North American transect. Remote Sensing of Environment, 137, 94–111. https://doi.org/10.1016/j.rse.2013.06.004

Hudak, A. T., Fekety, P. A., Kane, V. R., Kennedy, R. E., Filippelli, S. K., Falkowski, M. J., Tinkham, W. T., Smith, A. M. S., Crookston, N. L., Domke, G. M., Corrao, M. V., Bright, B. C., Churchill, D. J., Gould, P. J., McGaughey, R. J., Kane, J. T., & Dong, J. (2020). A carbon monitoring system for mapping regional, annual aboveground biomass across the northwestern USA. Environmental Research Letters, 15(9), 095003.

Huete, A., Didan, K., Miura, T., Rodriguez, E. P., Gao, X., & Ferreira, L. G. (2002). Overview of the radiometric and biophysical performance of the MODIS vegetation indices. Remote Sensing of Environment, 83(1), 195–213. https://doi.org/10.1016/S0034-4257(02)00096-2

Huete, A. R. (1988). A soil-adjusted vegetation index (SAVI). Remote Sensing of Environment, 25(3), 295–309. https://doi.org/10.1016/0034-4257(88)90106-X

Hyde, P., Dubayah, R., Walker, W., Blair, J. B., Hofton, M., & Hunsaker, C. (2006). Mapping forest structure for wildlife habitat analysis using multi-sensor (LiDAR, SAR/InSAR, ETM+, Quickbird) synergy. Remote Sensing of Environment, 102(1), 63–73. https://doi.org/10.1016/j.rse.2006.01.021

Jordan, C. F. (1969). Derivation of Leaf-Area Index from Quality of Light on the Forest Floor. Ecology, 50(4), 663–666. https://doi.org/10.2307/1936256

Kolden, C. A., Lutz, J. A., Key, C. H., Kane, J. T., & van Wagtendonk, J. W. (2012). Mapped versus actual burned area within wildfire perimeters: Characterizing the unburned. Forest Ecology and Management, 286, 38–47. https://doi.org/10.1016/j.foreco.2012.08.020

Kross, A., McNairn, H., Lapen, D., Sunohara, M., & Champagne, C. (2015). Assessment of RapidEye vegetation indices for estimation of leaf area index and biomass in corn and soybean crops. International Journal of Applied Earth Observation and Geoinformation, 34, 235–248. https://doi.org/10.1016/j.jag.2014.08.002

Kwak, D.-A., Lee, W.-K., Lee, J.-H., Biging, G. S., & Gong, P. (2007). Detection of individual trees and estimation of tree height usinkwakg LiDAR data. Journal of Forest Research, 12(6), 425–434. https://doi.org/10.1007/s10310-007-0041-9

Leckie, D., Gougeon, F., Hill, D., Quinn, R., Armstrong, L., & Shreenan, R. (2003). Combined high-density lidar and multispectral imagery for individual tree crown analysis. Canadian Journal of Remote Sensing, 29(5), 633–649. https://doi.org/10.5589/m03-024

Lehtonen, A., Mäkipää, R., Heikkinen, J., Sievänen, R., & Liski, J. (2004). Biomass expansion factors (BEFs) for Scots pine, Norway spruce and birch according to stand age for boreal forests. Forest Ecology and Management, 188(1), 211–224. https://doi.org/10.1016/j.foreco.2003.07.008

Lu, D. (2005). Aboveground biomass estimation using Landsat TM data in the Brazilian Amazon. International Journal of Remote Sensing, 26(12), 2509–2525. https://doi.org/10.1080/01431160500142145

Lu, Dengsheng, Chen, Q., Wang, G., Liu, L., Li, G., & Moran, E. (2016). A survey of remote sensing-based aboveground biomass estimation methods in forest ecosystems. International Journal of Digital Earth, 9(1), 63–105. https://doi.org/10.1080/17538947.2014.990526

Lu, Dengsheng, Chen, Q., Wang, G., Moran, E., Batistella, M., Zhang, M., Vaglio Laurin, G., & Saah, D. (2012). Aboveground Forest Biomass Estimation with Landsat and LiDAR Data and Uncertainty Analysis of the Estimates. International Journal of Forestry Research, 2012. https://doi.org/10.1155/2012/436537

Merzlyak, M. N., Gitelson, A. A., Chivkunova, O. B., & Rakitin, V. Y. (1999). Non-destructive optical detection of pigment changes during leaf senescence and fruit ripening. Physiologia Plantarum, 106(1), 135–141. https://doi.org/10.1034/j.1399-3054.1999.106119.x

Mutanga, O., & Skidmore, A. K. (2004). Narrow band vegetation indices overcome the saturation problem in biomass estimation. International Journal of Remote Sensing, 25(19), 3999–4014. https://doi.org/10.1080/01431160310001654923

Navarro, G., Caballero, I., Silva, G., Parra, P.-C., Vázquez, Á., & Caldeira, R. (2017). Evaluation of forest fire on Madeira Island using Sentinel-2A MSI imagery. International Journal of Applied Earth Observation and Geoinformation, 58, 97–106. https://doi.org/10.1016/j.jag.2017.02.003

Pandit, S., Tsuyuki, S., & Dube, T. (2018). Estimating Above-Ground Biomass in Sub-Tropical Buffer Zone Community Forests, Nepal, Using Sentinel 2 Data. Remote Sensing, 10(4), 601. https://doi.org/10.3390/rs10040601

Roteta, E., Bastarrika, A., Padilla, M., Storm, T., & Chuvieco, E. (2019). Development of a Sentinel-2 burned area algorithm: Generation of a small fire database for sub-Saharan Africa. Remote Sensing of Environment, 222, 1–17. https://doi.org/10.1016/j.rse.2018.12.011

Sharma, L. K., Bu, H., Denton, A., & Franzen, D. W. (2015). Active-Optical Sensors Using Red NDVI Compared to Red Edge NDVI for Prediction of Corn Grain Yield in North Dakota, U.S.A. Sensors, 15(11), 27832–27853. https://doi.org/10.3390/s151127832

Sims, D. A., & Gamon, J. A. (2002). Relationships between leaf pigment content and spectral reflectance across a wide range of species, leaf structures and developmental stages. Remote Sensing of Environment, 81(2), 337–354. https://doi.org/10.1016/S0034-4257(02)00010-X

Steininger, M. K. (2000). Satellite estimation of tropical secondary forest above-ground biomass: Data from Brazil and Bolivia. International Journal of Remote Sensing, 21(6–7), 1139–1157. https://doi.org/10.1080/014311600210119

Tucker, C. J. (1979). Red and photographic infrared linear combinations for monitoring vegetation. Remote Sensing of Environment, 8(2), 127–150. https://doi.org/10.1016/0034-4257(79)90013-0

Underwood, E. C., Ustin, S. L., & Ramirez, C. M. (2007). A Comparison of Spatial and Spectral Image Resolution for Mapping Invasive Plants in Coastal California. Environmental Management, 39(1), 63–83. https://doi.org/10.1007/s00267-005-0228-9

Wang, G., Zhang, M., Gertner, G. Z., Oyana, T., McRoberts, R. E., & Ge, H. (2011). Uncertainties of mapping aboveground forest carbon due to plot locations using national forest inventory plot and remotely sensed data. Scandinavian Journal of Forest Research, 26(4), 360–373. https://doi.org/10.1080/02827581.2011.564204